J Neurophysiol 97: 3684–3695, 2007.
First published March 21, 2007; doi:10.1152/jn.00886.2006.

Comparison of Direction and Object Selectivity of Local Field Potentials and Single Units in Macaque Posterior Parietal Cortex During Prehension

Itay Asher,[1,2] Eran Stark,[1] Moshe Abeles,[1,2,3] and Yifat Prut[1,2]

[1]*Department of Physiology, Hadassah Medical School and* [2]*The Interdisciplinary Center for Neural Computation, The Hebrew University of Jerusalem, Jerusalem; and* [3]*Gonda Brain Research Center, Bar Ilan University, Ramat-Gan, Israel*

Submitted 19 August 2006; accepted in final form 14 March 2007

Asher I, Stark E, Abeles M, Prut Y. Comparison of direction and object selectivity of local field potentials and single units in macaque posterior parietal cortex during prehension. *J Neurophysiol* 97: 3684–3695, 2007. First published March 21, 2007; doi:10.1152/jn.00886.2006. Recent studies have shown that the local field potential (LFP) can provide a simple method for obtaining an accurate measure of reaching and saccade behaviors. However, it is not clear whether this signal is equally informative with respect to more complex movements. Here we recorded LFPs and single units (SUs) from different areas in the posterior parietal cortex of macaques during a prehension task and compared LFP selectivity with SU selectivity. We found that parietal LFPs were often selective to target direction or object and that percentages of selective LFPs were similar to percentages of selective SUs. Nevertheless, SUs were more informative than LFPs in several respects. Preferred directions and objects of LFPs usually deviated from a uniform distribution, unlike preferences of SUs. Furthermore, preferences of LFPs did not reflect preferences of SUs even when the two signals were recorded simultaneously via the same electrode. Additionally, selectivity of movement-evoked LFPs appeared only after movement onset, whereas SUs frequently showed premovement selectivity. Spectral analysis revealed a lower signal-to-noise ratio of the LFP signal. Different frequency bands derived from a single LFP site showed inconsistent preferences. Significant relations with target parameters were found for all tested bands of LFP, but effects in the fast (gamma) band exhibited properties that were consistent with contamination of the LFP by residual spiking activity. Taken together, our results suggest that the LFP provides a simple method for extracting ample movement-related information. However, some of its properties make it less adequate for predicting rapidly changing movements.

INTRODUCTION

Prehension is a complex, multi-joint arm movement that involves coordinated reaching and grasping (Jeannerod 1984). Prehension movements are known to be planned and controlled by multiple brain areas, including various subdivisions of motor and parietal cortex. Most electrophysiological studies of reaching and grasping in macaques have examined firing rates of single units. Recently, several groups also examined local field potential (LFP) recorded during reaching and saccade tasks. The LFP is thought to reflect the summation of synaptic currents from a radius of up to a few millimeters (Mitzdorf 1985). As such, the LFP signal may provide a robust measure of activity within local cell assemblies (Engel et al. 2001). Furthermore, recording of LFP signals is usually simpler and more stable over time compared with single-unit (SU) recordings, and hence the LFP has been suggested as an input for brain-machine interfaces (Andersen et al. 2004). However, a key issue in characterizing the LFP and its possible clinical utility is its relative selectivity to perceptual and behavioral parameters compared with the selectivity of SU firing rates.

When estimating behavioral correlates of SU activity, the most commonly used parameter is neuronal firing rate. In contrast, a variety of temporal and spectral methods have been employed for quantifying the LFP signal and deciphering the relations between this signal and behavior. One approach is computing the evoked potential (EP), which reflects activity that is locked to sensory (Eggermont and Mossop 1998) or motor (Donchin et al. 2001; Mehring et al. 2003; Rickert et al. 2005) events. An alternative approach uses spectral analysis of LFP (Pesaran et al. 2002; Rickert et al. 2005; Scherberger et al. 2005) for studying behavior-related changes in the frequency content of the signal. This approach is better suited for characterizing oscillatory phenomena that are not phase-locked to behavioral events. These two approaches were recently combined (O'Leary and Hatsopoulos 2006) to characterize EPs of different frequency bands of the LFP. Applying these methods revealed significant relations between the LFP signal and task parameters. However, some studies (Mehring et al. 2003; Pesaran et al. 2002) have found the LFP signal to be at least as informative as the SU signal, whereas others (O'Leary and Hatsopoulos 2006; Scherberger et al. 2005) have reported several disadvantages of the LFP, such as a nonuniform distribution of directional preferences.

In the present study, we trained macaques to perform a delayed prehension task involving reaching and grasping objects. We examined simultaneously recorded neural activity in multiple areas within the posterior parietal cortex (PPC) and compared the selectivity of SUs and LFPs to target direction and object using similar analytical tools.

METHODS

Subjects

Two monkeys (*Macaca fascicularis*, females, *D* and *J,* 2.5/3.2 kg, respectively) were used in this study. Monkeys used the right hand for task performance, and recordings were made from the contralateral hemisphere. All surgical and animal handling procedures were according to the *National Institutes of Health Guide for the Care and Use of Laboratory Animals* (1996), complied with Israeli law, and were approved by the Ethics Committee of the Hebrew University.

Address for reprint requests and other correspondence: I. Asher, Dept. of Physiology, The Hebrew University, Hadassah Medical School, P.O. Box 12272, Jerusalem 91120, Israel (E-mail: itaya@ekmd.huji.ac.il).

The costs of publication of this article were defrayed in part by the payment of page charges. The article must therefore be hereby marked "*advertisement*" in accordance with 18 U.S.C. Section 1734 solely to indicate this fact.

Animal care was supervised by the veterinarian staff of the Hebrew University.

Behavioral setup and protocol

During task performance, the monkeys sat in a primate chair in a dark, sound-proof chamber. The workspace center was situated ~10 cm in front of the monkey. During training and recording sessions, the left arm was restrained. Monkeys were trained to reach, grasp, and hold three different objects presented at six equally spaced directions in the horizontal plane (Fig. 1*A*). All objects required a similar orientation of the shoulder, elbow, and wrist joints when presented in a given direction but different finger configurations for correct grip. Two microswitches located on each object ensured proper grasping. A touch pad (5.5 × 2 cm) was located in front of the monkey at the center of the workspace and at the same height as the horizontal target plane. On the touch pad three keys (1.3 × 1.3 cm) with red-green light-emitting diodes (LEDs) were installed (Fig. 1), and the monkey had to press the center key and not the other two. This resting position permitted movements of equal amplitude with minimal elevation changes, in all six directions (6.5/7.5 cm, *monkey D/J;* different amplitudes were used to accommodate differences in length of the monkeys' arms). A horizontal half-mirror was placed between the workspace (touch pad and objects) and the monkey's head. The half mirror prevented eye contact with the workspace at all times except a brief period of object presentation during which a light located below the half mirror was turned on. Thus during movement, the monkey did not see its hand or the target object, which had to be memorized during the delay. Great care was taken to ensure that dark adaptation was not possible (by turning the light on in the booth between blocks), and that the visual go signal did not allow the monkey to see the target object.

A trial was initiated when a green LED located on the central key of the touch pad turned on, cueing the monkey to press this key. After a variable control period (500–1,000 ms), an object was made visible to the monkey for a brief period (200–400 ms) and then obscured, by changing lighting conditions in the recording booth. After a variable delay (1,000–1,500 ms), a visual go signal was given (all LEDs illuminated in orange), and the monkey released the touch pad, reaching to grasp the object. Reaction time (from go signal to movement onset) was limited to 500/1,000 ms (*monkey D/J*), movement time (from movement onset to full grasp) was limited to 1,000/2,000 ms, and holding of the object was required for a variable period of 580–620/700-1,000 ms. The trial ended when the monkey, on visual cue, released the object and returned its hand to the touch pad. A drop of juice rewarded correct accomplishment of a trial. Trials were separated by an intertrial interval of 2–3 s and were arranged in blocks of 15 trials/block.

During each session, two objects were used. In most sessions, one object required a power-grip hand configuration, and the other required a precision grip. In some of the sessions, a third object, grasped by finger opposition, was used instead of the power grip object. Target direction assignment to trial was pseudo-randomized, such that objects were presented an approximately equal number of times in different directions.

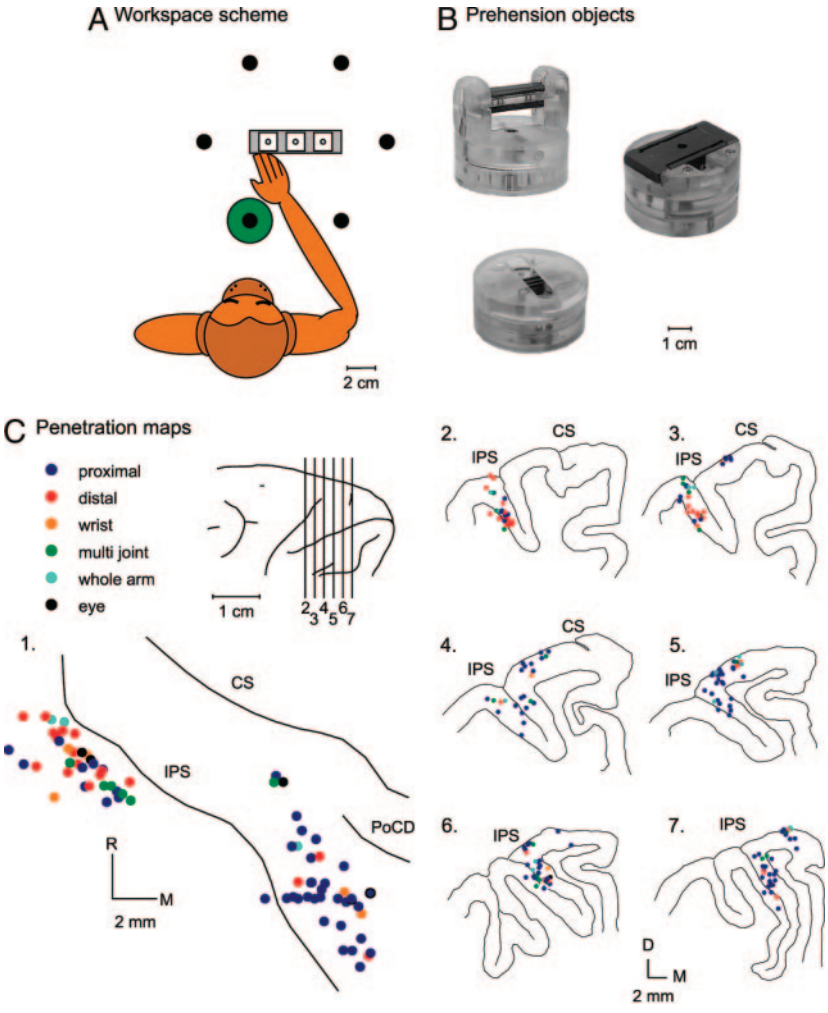

FIG. 1. Experimental setup and recording sites. *A*: schematic drawing of the workspace, top view. Objects were presented at 6 equally spaced directions in the horizontal plane, around a touch pad with 3 keys with red/green light-emitting diodes (LEDs). *B*: prehension objects. *Top*: power grip object, grasped by opposing palm and 4 fingers. *Bottom*: precision grip object, grasped with index and thumb. *Right*: finger opposition object, grasped by opposing thumb and 4 fingers. Scale bar is 1 cm. Microswitches located on objects ensured consistent grasping configuration. *C*: penetration maps. Surface map of left parietal cortex, *monkey J* (*left*), and coronal sections of left parietal cortex, *monkey D* (*right*), arranged from rostral to caudal in 2 mm intervals. *Inset*: location of sections. Sulci were reconstructed from MRI scans. Each circle corresponds to a penetration site of 1 electrode, colors indicate sensorimotor mapping results. CS, central sulcus; D, dorsal; IPS, intra-parietal sulcus; M, medial; PoCD, postcentral dimple; R, rostral.

Surgical procedures

Chamber implant surgeries were performed in aseptic conditions and under general anesthesia [isoflurane and N_2O, induced by ketamine (3 mg/kg) and medetomidine hydrochloride (Domitor, 0.1 mg/kg)]. During surgery, a piece of bone was removed above the motor and parietal cortices of the left hemisphere. Titanium screws were implanted in adjacent skull locations and a 44 × 22-mm plastic chamber was placed over the drilled hole. The chamber was then cemented to the skull using dental acrylic. Analgesics [pentazocine (Talwin), carprofen (Rymadil)] and antibiotics (ceftriaxone) were used pre- and postoperatively.

Prior to implant surgery, monkeys were anesthetized with ketamine-Domitor anesthesia, and water-filled glass beads were glued to the skull surface, using dental acrylic. Consecutive coronal MRI images (Biospec Bruker 4.7 T animal system, fast spin echo sequence; effective echo time, 80 ms; repetition time, 2.5 s; 0.5 × 0.5 × 2-mm resolution) showed the location of cortical landmarks relative to the beads and allowed for optimal positioning of the recording chamber. Additional MRI scans were conducted after chamber implantation (both monkeys), and postmortem (*monkey D* only). After completion of experiments, monkeys were deeply anesthetized (ketamine, pentobarbital, 30 mg/kg) and killed by an overdose of pentobarbital. During this procedure, pins were inserted in defined chamber locations to allow reconstruction of penetration sites relative to cortical landmarks.

Neural and behavioral recordings

During each session, 16 glass-coated tungsten micro-electrodes (impedance 0.2–2 MΩ at 1 kHz) were individually inserted into two cortical areas of the left hemisphere (EPS 1.31, Alpha-Omega Engineering, Nazareth, Israel). Electrodes were arranged in two independently positioned circular guide tubes (Double MT, Alpha-Omega Engineering, 1.5 mm ID, interelectrode spacing within each tube ~300 μm). The continuous signal from each electrode was amplified (10,000), band-pass filtered (1–10,000 Hz), and sampled at 25 kHz (Alpha-Map 5.4, Alpha-Omega Engineering). This signal was used for off-line spike and LFP extraction. Behavioral events were sampled at 6 kHz.

Neuronal activity was recorded from four parietal areas previously reported to be involved in reaching or grasping. Two subdivisions of the superior parietal lobule (SPL), medial intra-parietal area (MIP) (Snyder et al. 1997) and Area 5 (Ashe and Georgopoulos 1994) have been related to reaching. Two subdivisions of the inferior parietal lobule (IPL), anterior intra-parietal area (AIP) (Murata et al. 1996), and area 7b (Gardner et al. 1999) have been related to grasping. Anatomical identification of recording sites was based on MRI scans. Additionally, prior to the recording period, the cortical surface was mapped by testing the responses of local spiking activity to passive movement of limb joints, light stroking of the skin, and palpation of muscles as well as response to active prehension movements and saccades. This procedure was repeated at the end of each recording session. Rostral IPL recordings focused on locations anterior to the lateral intraparietal area (where saccade-related activity was observed), and posterior to finger areas of primary somatosensory area (Murata et al. 1996). SPL recordings focused on locations posterior to arm representations of primary somatosensory area and lateral to the postcentral dimple. The depth of each recording site relative to the surface of the cortex was used to determine whether the electrode tip was recording from a gyrus area (Areas 5 and 7b) or from a peri-sulcal area (MIP and AIP). Sites located at depths >2.5 mm were considered as recordings from a sulcus bank area provided their location matched a sulcus vicinity based on the MRI scans. This criterion used a typical macaque cortex thickness found during mapping and recording sessions in gyral areas.

Neural data preprocessing

Contaminations from the AC power line were removed from the continuous signal using pulse-triggered averaging, which provided the average interference. This waveform was subtracted from the original signal and updated in an adaptive manner. Spikes were sorted using principal component analysis-based software (Alpha-Sort 4.0, Alpha-Omega Engineering). Separation quality of sorted units was graded by interspike interval histograms, individual spike shapes, and cluster overlap. Trial-to-trial consistency of the responses was determined for each unit (using an algorithm based on a time-varying Poisson counting process) and validated by visual inspection of raster plots. Only well isolated units that had at least five trials per behavioral condition were included in SU analyses.

LFP was extracted by band-pass (1–100 Hz, 2-pole Butterworth) filtering and down-sampling to 500 Hz. Correct trials were realigned and cut by behavioral epochs (see following text). Outlier trials were detected and removed using a moving average of the root mean square (RMS, window length = 20 ms; 2.58 SDs threshold). These trials constituted <3% of all recorded trials. Only sites with at least five stationary LFP trials per behavioral condition, and in which spiking activity was recorded (minimal average rate 1 spike/s over the whole trial), were included in analyses.

The EP wave (average over traces) and its parametric confidence intervals (based on SE) were computed. Analyses included EPs computed by aligning LFP traces on three behavioral events: trial start (used as control), object presentation (visual-evoked potential, VEP), and movement onset (motor-evoked potential, MEPs, Fig. 2). The optimal alignment for MEPs was movement onset rather than the go signal (Rickert et al. 2005) or the grasp events. Other behavioral events tested, e.g., turning the visual cue off, typically did not reveal a significant EP.

Multi-taper spectral analysis (NFFT = 256 samples, frequency resolution: 1.95 Hz, 5 Slepian data tapers) was applied to each epoch in each trial. The multi-taper technique (Mitra and Pesaran 1999) was chosen because it provides a formal method to obtain estimates of the spectrum with optimal bias and variance properties. Next, the power in frequency bands was summed for each epoch and trial. Frequency bands were defined as follows: delta (1–4 Hz), theta (4–8 Hz), alpha (8–13 Hz), beta (13–30 Hz), lower gamma (30–60 Hz), and higher gamma (60–100 Hz). Because results for delta, theta, and alpha frequency bands were very similar, data are presented below as a single band, 1–13 Hz.

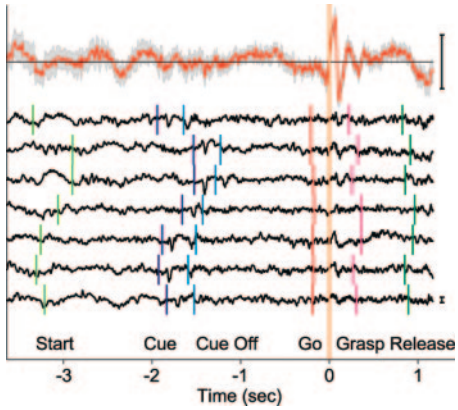

FIG. 2. Field potential traces and motor-evoked potential (MEP) recorded from anterior intra-parietal cortex. Averaging is based on 38 repetitions of the same condition (power-grip object, direction 60°), of which only the 1st 7 traces are shown, aligned on movement onset. Note different scales for raw traces and average (each scale bar is 50 μV; MEP is magnified 10 times relative to single trials). Confidence interval around the MEP (gray shading) is ±1.96 SE (computed for each sample point). Vertical marks indicate behavioral events. The visual-evoked potential (VEP) is also evident in the single trials but not in the average trace because of misalignment.

Data analysis

Seven behavioral epochs (each 400 ms long) were defined as follows. *1*) *Control epoch* (CE): 100–500 ms after trial start. During this epoch, the monkey's hand continuously pressed the central button of the touch pad, and the monkey had no information on the behavioral condition of the trial. *2*) *Signal*: 50–450 ms after object presentation. During this epoch, the monkey's hand pressed the central button of the touch pad, and the monkey had visual information on the behavioral condition of the trial. The object was visible for the first 150–350 ms of this epoch. *3*) *Set1*: 450–850 ms after object presentation. Hand configuration was the same as during the control and signal epoch, but the target was not visible to the monkey. *4*) *Set2*: 850–1250 ms after object presentation. All behavior and stimulus conditions were the same as for set1. *5*) *Pre-Go*: 400–0 ms before the go signal. All behavior and stimulus conditions were the same as for set1. On average, there was a 100 ms overlap between this epoch and epoch set2. Hereafter, the latter three epochs (set1, set2, and pre-Go) are referred to as "delay epochs." *6*) *Reaction and Movement time* (RTMT): 150 ms before to 250 ms after movement onset (defined as touch pad release). *7*) *Hold:* 100–500 ms after object grasp. During this epoch, the monkey's hand constantly gripped the object.

Direction and object selectivity of different neuronal signals

Directional tuning curves of SUs were computed by averaging the spike counts in each direction (pooling trials from 2 objects). Tuning curves were computed for each behavioral epoch separately. Similarly, a preferred object was identified by pooling trials from all six directions. The selectivity of units to target parameters was tested using a two-way test for direction, object and interaction effects, separately for each behavioral epoch (Kruskal-Wallis test, $\alpha = 0.01$).

Vector summation was used to estimate the preferred direction (PD), which is the angle of the vector sum and the normalized length of the vector sum (r) (Mardia 1972) which could vary between zero (nonselective to direction) and one (response only to 1 direction). Resampling methods (Stark and Abeles 2005) were used to compute a confidence interval around each PD. We then tested the fit of the obtained tuning curve to a von Mises model that provides a parametric tuning function. The von Mises tuning function is described by the term

$$f(\theta) = m + \frac{s}{2\pi I_0(\kappa)} e^{\kappa\cos(\theta-\mu)}$$

$f(\theta)$, the predicted response in direction θ; m, the baseline response; s, gain; μ, preferred direction; κ, tuning width; I_0; modified Bessel function of the first kind and order zero.

An observed tuning curve was considered well described by the von Mises model if the regression test yielded a P value <0.01 ($R^2 > 0.84$). For such tuning curves, the width was quantified using the half-width at half height, which is a transformation of the estimated width parameter κ (Amirikian and Georgopoulos 2000). Henceforth, we refer to a signal as *directionally tuned*, only if it was direction-selective *and* its tuning curve was well described by a von Mises model. Analyses of PD distributions and PD differences were restricted to directionally tuned signals.

Directional tuning curves of EPs were computed by pooling trials from two objects in each direction and averaging the aligned traces, yielding six EPs. The RMS amplitude of each EP was computed, yielding a six-element tuning curve. Note that the properties of the EP wave (amplitude, spectral content, etc.) depend on the properties of single-trial traces as well as on the degree of their phase-locking. Thus the amplitude of the EP in a given direction does not equal the average amplitude of single trials in this direction. Subsequently, the EP tuning curve in our experiment is a six-element vector of EP amplitudes rather than six averages (with 6 variances) of single-trial amplitudes. An ANOVA-type statistical test such as the Kruskal-Wallis (which was used for estimating SU selectivity) cannot be used for testing EPs. We therefore used resampling methods (Crammond and Kalaska 1996; Georgopoulos et al. 1988; Stark and Abeles 2005) to test the significance of EP selectivity. The significance test for directional selectivity involved 1,000 repetitions of a shuffling procedure in which traces of single trials were randomly reassigned to different movement directions, six EPs were computed, and the normalized length of the vector sum (r) was recomputed. A channel was considered directionally selective if the length of the true vector sum exceeded $\geq$990 of the 1,000 shuffled lengths (1-tailed test, $P < 0.01$). Object selectivity was tested by pooling across reaching directions and comparing the true difference between two EP amplitudes with 1000 differences between shuffled amplitudes (2-tailed test, $P < 0.01$).

Analysis of LFP power selectivity was essentially identical to that used for SUs (see preceding text). However, in this case, instead of the spike count in a given trial and epoch, the estimated power in each frequency band was considered the dependent variable. Thus each LFP site was tested four times in each epoch (for band ranges of 1–13, 13–30, 30–60, and 60–100 Hz). PD differences across different frequency bands of the LFP recorded from the same site involved a resampling test for equality of PDs (Stark and Abeles 2005).

To compare selectivity of different signals, it was necessary to use the same measures and tests. Therefore in analyses that involved comparisons between EPs and SUs, we applied the resampling tests to SU data. On the other hand, the Kruskal-Wallis test was used when comparing selectivity of SUs to selectivity of LFP power. Nevertheless, in our data the two tests identified almost the same subsets of SUs as selective, hence providing similar percentages of selective SUs.

Distributions of preferred directions (computed for each cortical area, epoch, and signal type) were tested against the null hypothesis of uniform distribution, using Rao's test for equal spacing. Similarly, the overall object preference of a cortical area was tested against the null hypothesis of equal probability to prefer either object (binomial test).

In addition to testing tuning properties, we estimated the effect size using the η^2 measure (Fisher 1925), defined as the sum of squares of a given effect (direction, object, or interaction) divided by the total sum of squares, which includes the sums of squares of all three effects, and the error sum of squares (trial-by-trial variability unrelated to any effect). Thus the effect size (η^2) estimates the proportion of variance in the dependent variable that is attributable to each effect, and is therefore bounded between 0 and 1.

We quantified the association between the LFP signal and simultaneously recorded SUs by calculating the signal and noise correlation (Lee et al. 1998) for the 12 behavioral conditions, separately for each epoch. Second, we computed the absolute PD differences of directionally tuned signal pairs (ranging from 0 to 180°). Third, we quantified the temporal profile of each signal (unit firing or LFP in a certain band) as a seven-element vector where each element is the mean activity during one epoch, pooled over behaviors. We then estimated the correlation between these profiles using Spearman's rank correlation.

RESULTS

A total of 810 PPC SUs and 345 LFP sites, recorded in 43 sessions, were analyzed. Table 1 shows the distribution of SUs and LFP sites by monkeys and cortical areas. In the following subsections, population analyses compare pooled data of SPL (MIP and Area 5, so-called "reaching-related" areas) versus IPL (AIP and Area 7b, so-called "grasping-related" areas). Some differences between gyral areas (Areas 5 and 7b) and sulcal areas (MIP and AIP) were observed, but unless mentioned otherwise, these did not change the major findings presented in the following text. No significant differences between monkeys were observed, and therefore findings are presented pooled across monkeys.

TABLE 1. *Numbers of single units and LFPs by monkey and recording area*

	SPL		IPL		
Monkey/Area	MIP	Area 5	AIP	Area 7b	Total
Monkey D	183 (99)	195 (79)	171 (72)	49 (23)	598 (273)
Monkey J	39 (15)	80 (26)	78 (27)	15 (4)	212 (72)
Total	222 (114)	275 (105)	249 (99)	64 (27)	810 (345)

Parentheses enclose numbers of local field potential sites. SPL and IPL, superior and inferior parietal lobe; MIP and AIP, medial and anterior intraparietal area.

Direction and object selectivity of evoked field potentials

EPs computed for different directions and objects often revealed substantial modulation related to task parameters (Fig. 3*A*). Both VEPs and MEPs were often directionally selective (57.1 and 58.6%, respectively). The percentages of directionally selective EPs were similar to those of selective SUs (50.1 and 58.0%, Fig. 3*B*). The percentage of object selective LFPs was smaller than the percentage of direction selective LFPs (possibly due to the small number of objects used in each session) but significantly more frequent in MEPs than in SUs (37.7 vs. 15.6%, binomial test, $P < 0.01$). In contrast, EP selectivity was not higher than expected by chance (0.9% for direction and 1.6% for object) for EPs computed by averaging traces of the control epoch when the monkey was not moving and had no prior knowledge about target direction and object.

Next, we examined how many EPs and SUs were *directionally tuned*, that is direction selective *and* well described by a von Mises model. Typically, direction-selective SUs showed better fit to a von Mises model than EPs; 58.9 and 42.9% of the direction-selective VEPs/MEPs were well described by a von Mises model versus 69.6 and 66.8% of the tuned SUs (Fig. 3). One possible explanation for the better fit of SUs to a von Mises model is that more tuning curves of LFPs were actually bimodal and not unimodal as the von Mises distribution assumes. However, the number of reach directions used in this task was too small to test the fit of the data to a bimodal von Mises model (Amirikian and Georgopoulos 2000). The tuning widths of tuned EPs were similar to those of tuned SUs (Mann-Whitney test, $P > 0.01$ for both epochs). Mean tuning widths of tuned VEPs/MEPs were 46.5 ± 24.0/51.8 ± 21.0°, mean ± SD, respectively, whereas mean values for tuned SUs during the same time windows were 46.1 ± 19.2/51.2 ± 19.2°.

Preferred directions of VEPs and MEPs were not uniformly distributed as opposed to PDs of SUs (Fig. 4). For example, VEPs expressed under-representation of right-left directions (Rao's test, $P < 0.01$). Similarly, object-selective MEPs were also biased, showing a preference of the power grip object over the precision grip object (binomial test, $P < 0.01$). Furthermore, there was a great discrepancy, in terms of the preferred direction, between the tuning of EPs and the tuning of SUs

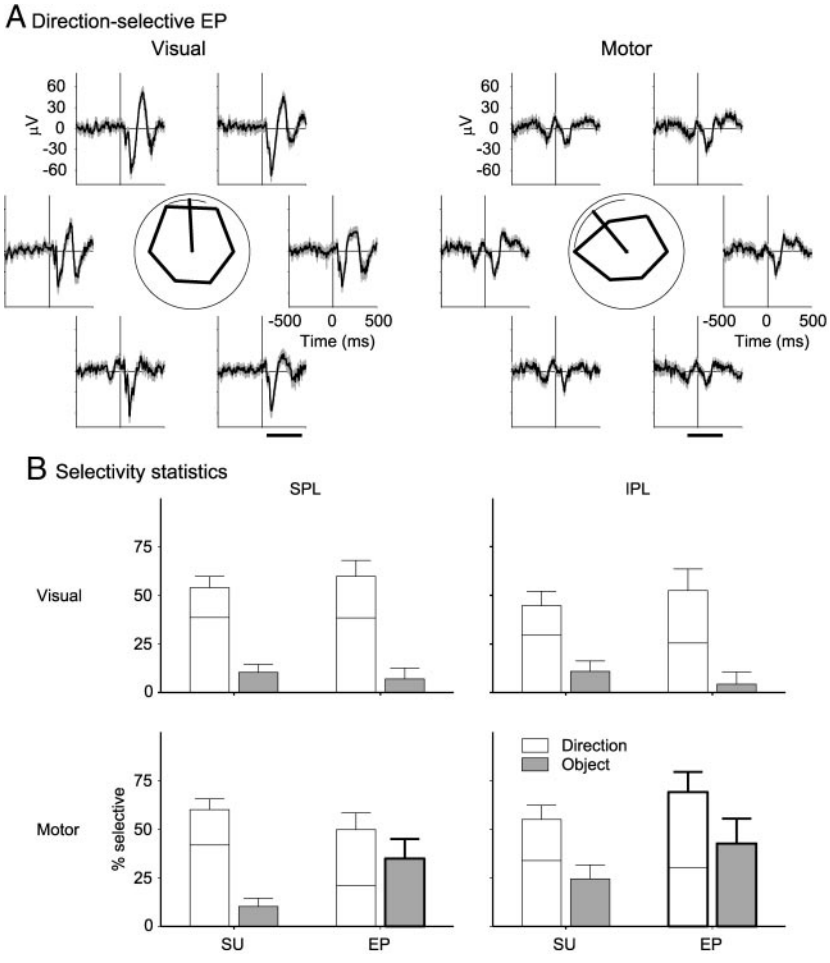

FIG. 3. Directional selectivity of visual and motor evoked potentials. *A*: VEPs (*left*) and MEPs (*right*) from 6 reaching directions (pooling trials from 2 objects) computed for an anterior intra-parietal area (AIP) site. Traces were aligned either on object presentation (VEP) or movement onset (MEP). Confidence intervals around evoked potential (EP) traces indicate ±1.96 SE. Horizontal bars indicate time windows used for computing the effect amplitude. *Insets*: polar tuning curves of EP amplitudes. The preferred direction is the angle of the vector sum of 6 responses. Arches denote confidence intervals around the preferred direction ($\alpha = 0.01$, resampling test). The radius of the circle corresponds to 32.8/18.5 μV. *B*: percentages of direction and object selective EP vs. percentages of selective single units (SUs), shown separately for superior parietal lobule (SPL, *left*) and inferior parietal lobule (IPL, *right*), and for VEPs (*top*) and MEPs (*bottom*). Plotted results are based on applying the same resampling tests for EP and SU data. In bars representing direction selectivity, the lower portions designate the percentage of directionally *tuned* EPs or SUs (see METHODS). Error bars are binomial confidence intervals ($\alpha = 0.01$). A bolded bar indicates that the proportion of direction or object selective EPs is significantly different from the corresponding proportion of selective SUs. Numbers of units and local field potential (LFP) sites are the same as in Table 1.

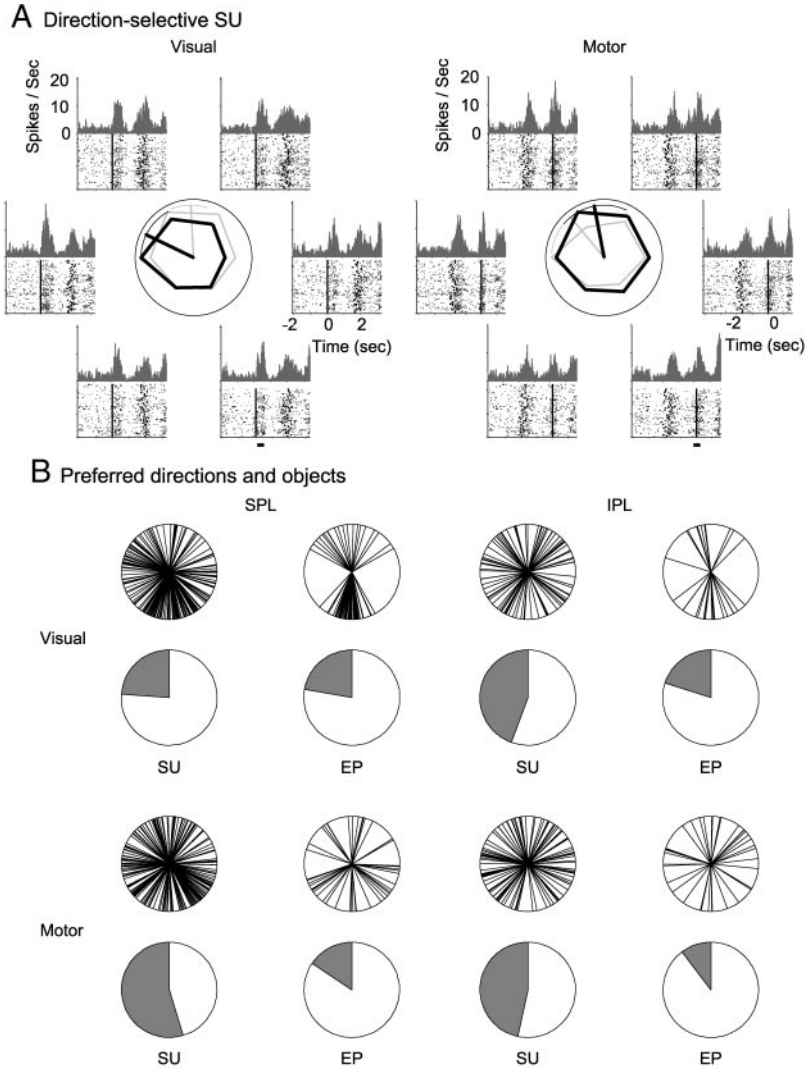

FIG. 4. Preferred directions and objects of EPs compared with SUs. *A*: raster plots, peri-event time histograms and polar plots of SU spikes recorded simultaneously with field potential in the same site and same behavioral conditions as in Fig. 3. Raster plots and histograms are aligned either on object presentation (*left*) or movement onset (*right*). Bolded vertical ticks on the spike raster plots indicate behavioral events: object presentation and movement onset. Horizontal bars indicate time windows used for computing effect amplitude. *Insets*: polar tuning curves of spike count amplitudes (black) are different from those of the EPs recorded in the same site (gray, taken from Fig. 3). Arches denote confidence intervals around the preferred direction ($\alpha = 0.01$, resampling test). The radius of the circle corresponds to 12.0/10.3 spike/s. *B*: distributions of preferred directions and objects of SUs and of EPs. For each area and epoch, distributions of significant preferred directions (PDs) and objects are displayed. Each spoke represents a single PD. Pie charts display percentages of units or sites that preferred power grip (white) or precision grip (gray). Analysis of preferred objects only used data recorded in sessions where the power grip and the precision grip objects were used. Plotted results are based on applying the same resampling tests for EP and SU data.

recorded by the same electrode. For sites in which *both* SU activity and the EP were tuned in the same epoch, the angular PD difference was computed. Mean PD differences were 56.7 ± 48.2 and 78.2 ± 50.1 for visual and motor tuning curves, respectively. Note that under the null hypothesis of independence between PD distributions the expected value is 90°.

We extended the parameter-selectivity analysis to multiple, partially overlapping, time windows around movement onset to compare the percentage of direction- and object-selective LFPs and SUs as a function of time. We found that directional selectivity of MEPs tended to emerge later than SU selectivity (Fig. 5*A*). SUs were often selective to target direction before movement onset. In contrast, MEPs computed from strictly premovement time windows were almost always uninformative. This finding was robust with respect to window duration. There was also a tendency for SUs (but not MEPs) to express object-selectivity before movement onset (Fig. 5*B*). However, this effect was weaker due to the small number of objects that were used (2 compared with 6 directions).

Task-dependent changes in the LFP spectrum

We analyzed the modulation of LFP spectral content during different epochs of the task. Parietal LFPs were dominated by frequencies <30 Hz regardless of behavioral epoch and anatomical location (Fig. 6*A*). However, the relative weight of the beta (13–30 Hz) band compared with slower frequencies depended on the behavioral epoch and the recording area (see following text). Power in the gamma band constituted only a small percentage of the total power. However, when compared with baseline power, it showed a consistent wide-band (30–100 Hz) increase during the task (Fig. 6*B*).

Quantifying the band-specific relative changes in power we found first that power in the slow frequency bands (<13 Hz) expressed inconsistent modulations. Generally, the slow frequencies power tended to decrease during the task especially during delay epochs (power decrease in 76.9%, increase in 6.0% of the sites). Nevertheless, in some cases, a power increase was observed during the signal, RTMT, and hold epochs, reflecting the occurrence of EPs at these times. Second, we found that previously reported beta oscillations (Scherberger et al. 2005) were site-specific. In our data, such oscillations were observed during delay (57.0%) and hold (80.7%) epochs in area MIP, whereas in the adjacent area 5, all epochs were characterized by a *decrease* in beta activity. Results in areas AIP and 7b were mixed. Last, power in the gamma range increased during the task in the majority (75.7%) of the

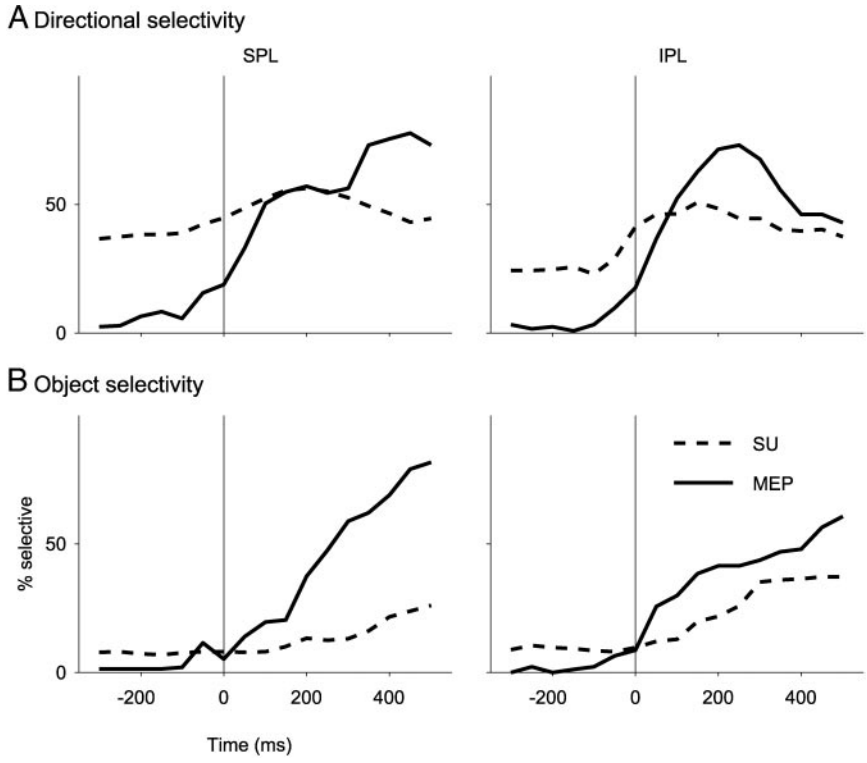

FIG. 5. Time course of direction and object selectivity. Percentages of direction- and object-selective MEPs (—) and SU activity (- - -) are plotted as a function of time relative to movement onset. Selectivity was tested in successive, partially overlapping time windows each of 200-ms duration and 50-ms time steps. Each time point was taken as the time of window end. Thus *time 0* indicates that the 200-ms window ends at movement onset. Each subplot corresponds to 1 cortical area. *A*: directional selectivity. *B*: object selectivity. Plotted results are based on applying the same resampling tests for EP and SU data.

recording sites and in all recorded areas. The increase in power of slow frequencies in "grasping areas" was much stronger in the "fast" monkey (*D*) than in the "slow" monkey (*J*). In contrast, in LFPs recorded from this monkey, beta oscillations were very prominent, even during the control epoch.

Direction and object selectivity of the LFP power spectrum

Computing the band-specific selectivity of LFPs revealed that selectivity to target direction and/or object was common in all frequency bands. Figure 7 displays the percentages of selective and tuned SUs as well as three different frequency bands. We found that percentages of direction and/or object selective LFP sites were similar to the percentages of selective SUs (with larger proportions of both LFPs and SUs selective to direction than to target object). Also, both LFPs and SUs were more likely to exhibit directional selectivity when the visual cue was presented, whereas object preference was most common during the hold epoch. Some anatomical differences were found in terms of the selectivity of different frequency bands (e.g., gamma power was most selective in Area 5, whereas beta power was most selective in MIP), but these differences were relatively small. Preferences (direction and/or object) of different bands in a given LFP site varied greatly (Fig. 8*A*). Mean PD differences between slow (1–13 Hz) and fast (60–100) components of LFPs were often not significantly different from the expected value under the assumption of independence (90°), yet the distributions of differences were typically bimodal (Fig. 8*B, left*). Adjacent bands in the LFP also expressed considerable, albeit smaller, PD differences. Minimal differences were observed between 30- to 60- and 60- to 100-Hz bands (Fig. 8*B, right*).

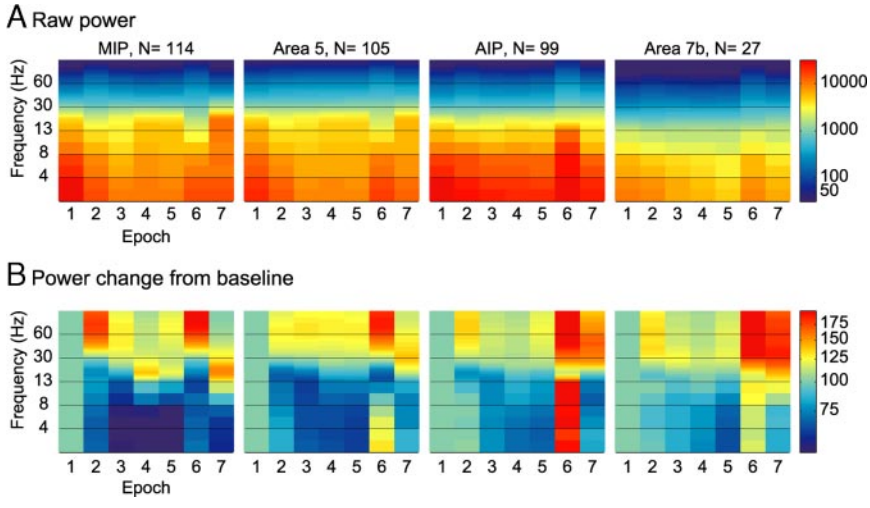

FIG. 6. Average LFP power spectra as a function of cortical area and behavioral epoch. Each spectrogram displays the average power spectrum of recording sites from 1 cortical area for 7 behavioral epochs (see METHODS). *A*: raw power given at μV^2. *B*: power ratio in each time and frequency bin relative to power during the control epoch, given as percent power. By definition, for the control epoch the ratio is 100% for all frequency bins. Thin horizontal lines separate the frequency bands used in the analysis (see METHODS). The frequency scale was adjusted such that each of the 6 frequency bands received equal weight (original frequency resolution: 1.95 Hz). Color scales are logarithmic for all plots. Epoch 1: control epoch, 2: signal epoch, 3: set1 epoch, 4: set2 epoch, 5: pre-Go epoch, 6: reaction and movement time (RTMT) epoch, 7: hold epoch.

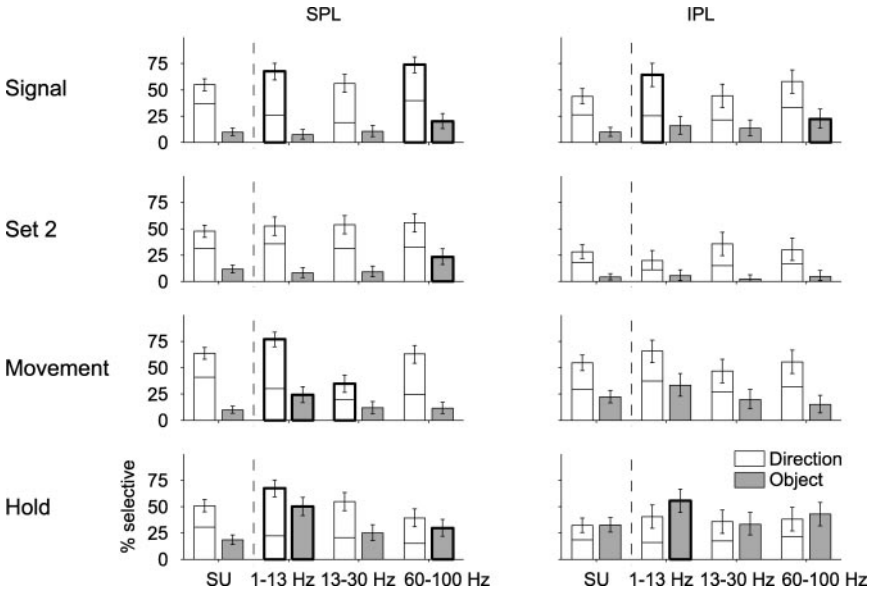

FIG. 7. Directional and object selectivity of SUs and LFP power. Each subplot displays percentages of direction- and object-selective LFPs vs. percentages of selective SUs, separately for SPL (*left*) and IPL (*right*) and for 4 behavioral epochs (rows). SUs are compared in each epoch to 3 frequency bands: slow (1–13 Hz), intermediate (13–30 Hz), and fast (60–100 Hz). In bars representing direction selectivity, the lower portions designate the percentage of directionally *tuned* LFPs or SUs (see METHODS). Error bars are binomial confidence intervals ($\alpha = 0.01$, corrected for multiple comparisons using the Dunn-Šidák method). A boldface bar indicates that the proportion of selective LFPs in a certain frequency band is significantly different from the corresponding proportion of selective SUs. Note that in all but one of these cases, LFPs were more likely to be selective than SUs. Plotted results are based on applying the same (Kruskal-Wallis) tests on LFP and SU data.

We found that PDs of LFP power often had nonuniform PD distributions (Fig. 9*A*) unlike SUs. The PD distributions of LFPs were biased toward far targets during the signal epoch, toward near targets during the delay epochs, and toward contra-lateral (right) directions during hold (beta and gamma bands, Rao's test, $P < 0.01$). Finally, we quantified the signal-to-noise ratio of LFPs using the η^2 effect size (Fisher 1925), which measures the response size relative to the trial-by-trial variability. SUs tended to have higher effect sizes than LFPs regardless of the frequency band (Fig. 9*B*).

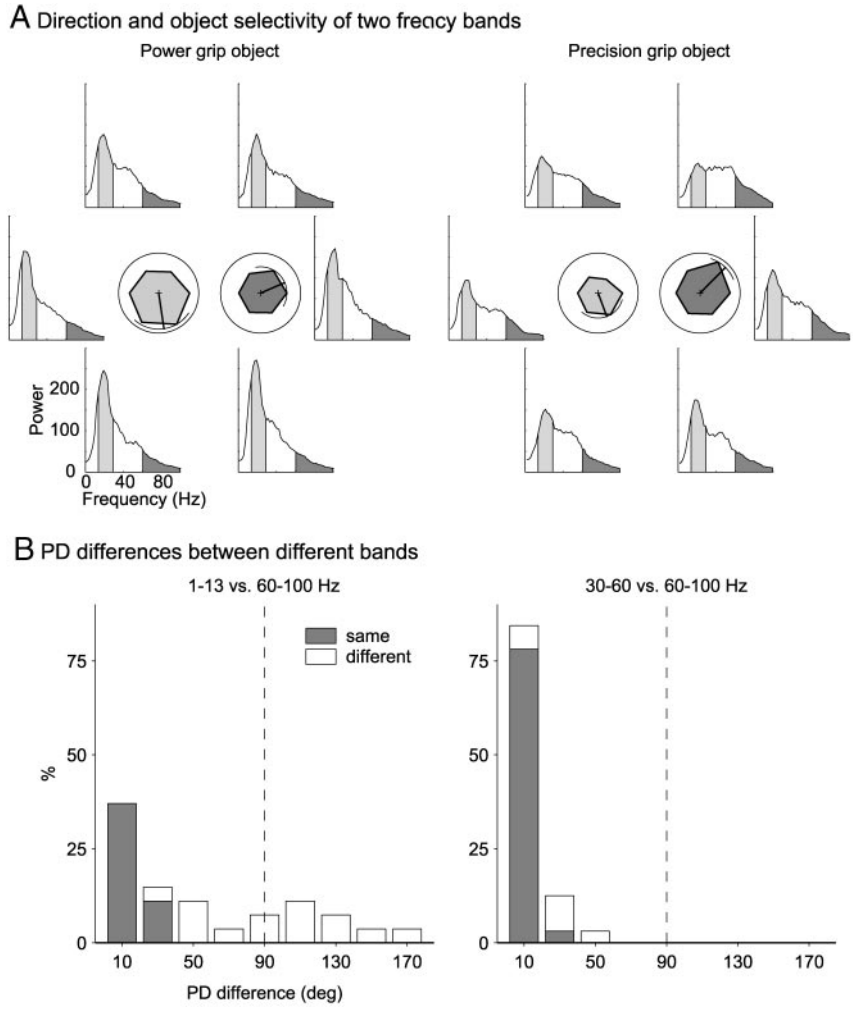

FIG. 8. Inconsistent preferences of different LFP bands. *A*: average power spectrum in a given direction and object (*left*: power grip object; *right*: precision grip object) for a single AIP recording during the hold epoch. Shaded areas mark the beta (light gray) and high-gamma (dark gray) frequency bands. *Insets*: polar tuning curves of the power, normalized (separately for each frequency band) by the maximal value over 12 conditions. The radius of the circle corresponds to 2,133/928 μV^2. *B*: PD differences between pairs of LFP frequency bands during the "set2" epoch. PD differences are shown for 2 band pairs: differences between PDs of the slow and the fast band (*left*) and differences between the 2 portions of the gamma band (*right*). Only sites in which *both* frequency bands were tuned were included in the analysis (left, $n = 32$; right: $n = 27$). A permutation test (see METHODS) was used to distinguish similar (gray) from different (white) PDs. The vertical dashed line represents the expected mean difference under the assumption of independence between bands.

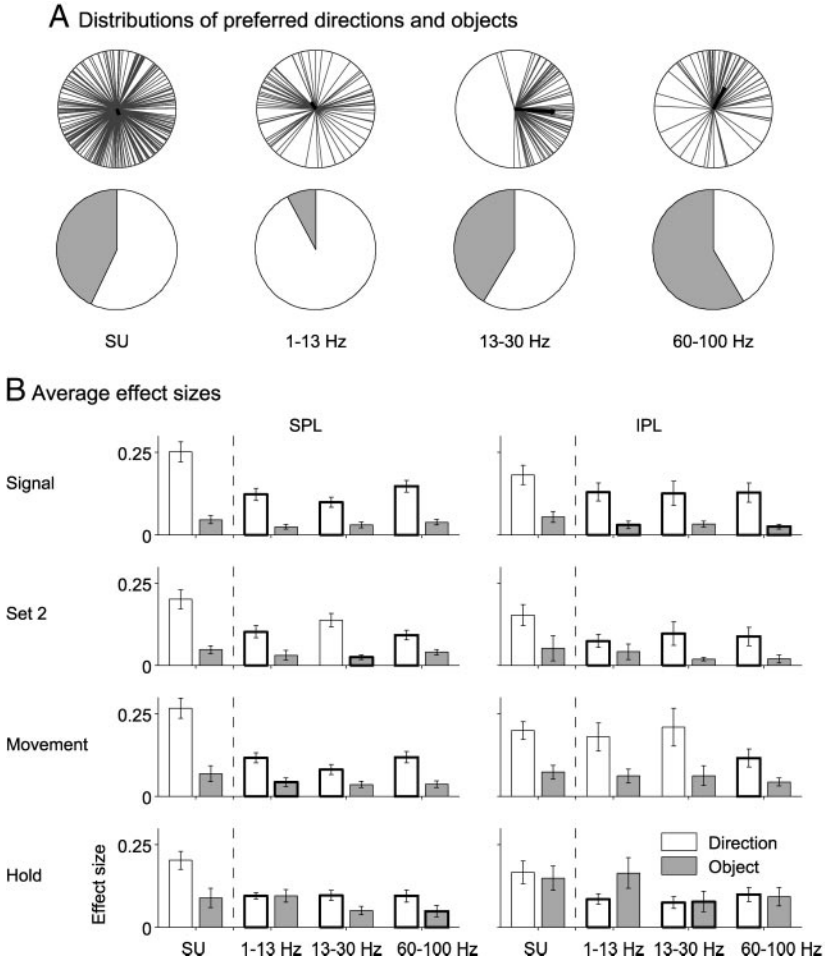

FIG. 9. Representation of task parameters by LFP spectra and SUs. *A*: distributions of significant preferred directions (*top*) and objects (*bottom*) during the hold epoch. Conventions are as used in Fig. 4. *B*: average direction and object effect sizes (η^2) of significantly selective units and LFP sites as a function of task epoch. Error bars are SE-based confidence intervals ($\alpha = 0.01$, corrected for multiple comparisons using the Dunn-Šidák method). A boldface bar indicates that effect size of selective LFPs in a certain frequency band is significantly different from the corresponding effect size of selective SUs (2-tailed Mann-Whitney test).

Relations between LFP gamma range and spike firing

Although the LFP was dominated by slow frequencies, we found a substantial increase in gamma (30–100) range power during the task compared with the control spectrum (Fig. 6*B*). We tested the relationship between gamma-band tuning and spike firing by computing the similarity of tuning curves between these two signals (i.e., signal correlation). A moderate but significant signal correlation was observed between tuning curves constructed from spike firing and tuning curves constructed for gamma power (Fig. 10*A*), whereas the average signal correlation was near zero for the slower (<30 Hz) frequency bands. The trial-to-trial co-variability (i.e., noise-correlation) between gamma power and neuronal firing rates was significantly higher than zero (Fig. 10*B*). In addition, the average response pattern of SUs was similar to the average changes in gamma power. For example, the increased SU firing during the signal and RTMT epochs characteristic of area MIP (Snyder et al. 1997) was accompanied by similar changes in gamma power (Fig. 6). To quantify this tendency, we computed the correlation between temporal profiles of firing rates and LFP power in each band (see METHODS, Fig. 10*C*). For slow frequency bands, the distribution of correlation coefficients was symmetric around zero. However, for gamma band frequencies the distributions of correlation coefficients were highly skewed toward values close to 1 (median $r = 0.57/0.75$, respectively), indicating that changes in firing rate co-occurred with an increase in the LFP power in gamma frequencies. This tendency was common to all examined cortical areas and was also evident when correlation coefficients were computed on a single trial basis.

Finally, spike-triggered averages of the LFP revealed no consistent phase relations between gamma band and firing times, suggesting that spikes are not phase-locked to gamma oscillations. Instead, averaging of LFPs around spike times of units recorded by the same site often showed a sharp feature at zero lag (Goldberg et al. 2004). Such features may suggest residuals of spike waveforms in the LFP signal despite the low-pass filtering used when acquiring this signal.

DISCUSSION

The main objective of this study was to examine the selectivity of posterior parietal LFPs during prehension to target direction and object and to compare these properties to those exhibited by SUs using similar analytical tools. We found that LFP in PPC was very often selective to target direction or object and that percentages of direction- or object-selective LFP sites were similar to or even higher than percentages of selective neurons. However, LFPs and SUs differed greatly in their tuning properties. The preferred directions and objects of LFPs were not uniformly distributed in contrast to the uniform distributions of SU preferences. Furthermore, LFP preferences did not reflect SU preferences even when the two signals were recorded simultaneously via the same electrode. In addition, selectivity of movement-evoked LFPs lagged behind the selec-

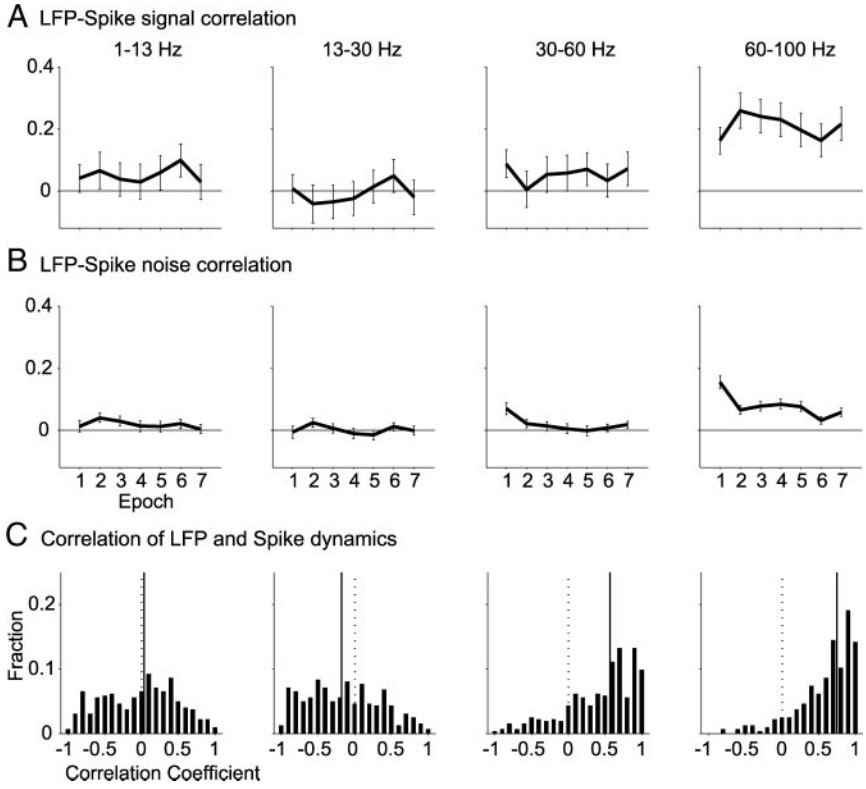

FIG. 10. Correlation analyses between LFP power and firing rates. Average signal (*A*) and noise (*B*) correlation between firing rates and LFP power as a function of task epoch in 3 frequency bands ($n = 324$ sites). Error bars are SE-based confidence intervals ($\alpha = 0.01$). *C*: distributions of rank correlation values computed between mean spike counts in different epochs and mean power in each frequency band ($n = 324$ sites). Vertical solid lines mark median values for each distribution.

tivity of SUs, appearing only after movement onset. Decomposing the LFP signal into different frequencies and studying the selectivity of LFP power provided essentially the same properties as those of EPs. Additionally, the spectral analysis revealed a lower signal-to-noise ratio of the LFPs compared with SUs and different frequency bands derived from a single LFP site showed inconsistent preferences.

Our results provide novel information concerning the selectivity of LFP to different behavioral parameters and the relations of LFP to local SU activity. Specifically, this report contains findings from parietal areas that were previously unexplored and in a complex task that combines reach and grasp. The general consistency of our results with studies of LFPs recorded in primary motor (Mehring et al. 2003; Rickert et al. 2005) and dorsal premotor cortex (O'Leary and Hatsopoulos 2006) suggests that these findings are robust and reflect general properties of the LFP behavior that is independent of the specific recording site and performed task.

Predicting movements using LFPs and SUs

We found that preferred directions of LFPs were nonuniformly distributed, consistent with previous reports of motor and parietal LFPs (O'Leary and Hatsopoulos 2006; Scherberger et al. 2005). Furthermore, object representation by LFPs was biased. This property may hinder reconstructing motor behavior from LFPs compared with SUs. An additional disadvantage of MEPs compared with SUs was their tendency to become selective to task parameters only after movement onset. A similar absence of premovement LFP selectivity was reported for primary motor cortex (Mehring et al. 2003; Rickert et al. 2005). This finding is especially surprising because many MEPs start ~100 ms before movement onset, namely during the reaction time (Donchin et al. 2001). Mitzdorf (1985) related early EP peaks to subcortical inputs and late peaks to local cortical feedback. Thus early activity observed in the EP might be related to inputs converging on this area that are insensitive to specific target properties (Roux et al. 2006) as opposed to cortical premovement processing. The lag of MEP selectivity after SU selectivity makes this signal unsuitable for predicting movement intention as required for some clinical applications. Adding a delay between cue onset and go signal may reveal early selectivity of VEPs (O'Leary and Hatsopoulos 2006), but this scenario is rarely encountered in natural movements. In contrast to EPs, premovement selectivity was frequently found when tuning curves were constructed from LFP power spectra (see also Rickert et al. 2005; Scherberger et al. 2005). As such, spectral-based analysis of LFP is a more suitable measure when movement prediction is required.

Finally, on our study as well as previous reports (Scherberger et al. 2005), the LFP signal (either evoked or spectrally analyzed) appears to be better suited for distinguishing between global parameters (such as reach vs. saccade in Scherberger et al.'s study or power vs. precision grip in our study). In this respect, the LFP is at least as good as or even better than SUs. However, its ability to distinguish between finely spaced variables (e.g., different directions of movement) is inferior to that of SUs. This may be related to the fact that each LFP site sums activity of a large population of neurons and thus averages out the fine details of neuronal activity.

LFP oscillations and their behavioral relevance

Although theoretical studies have stressed the utility of gamma oscillations for computations involving distributed cell assemblies and requiring high temporal acuity (e.g., von der

Malsburg and Buhmann 1992), we found considerable task-related changes in the slow components of the LFP (<13 Hz). Specifically, the power of slow frequencies in area AIP showed a prominent increase around and after movement (Fig. 6). Moreover, we found that slow frequencies contain ample information about target or movement properties, consistent with results obtained in motor cortex (O'Leary and Hatsopoulos 2006; Rickert et al. 2005). A recent report by Pesaran et al. (2005), who recorded LFP and SU activity simultaneously in area MIP and in dorsal premotor cortex, suggested that slow cortical rhythms may play a role in coordination *across* cortical areas; this is obviously required in complex motor tasks such as prehension. Therefore future empirical and theoretical studies of cortical oscillations should not be limited to gamma-range activity but rather focus on low-frequency oscillations as well (Kahana et al. 2001).

Specifically for the development of clinical applications, it is of great interest to compare the decoding power of slow LFP frequencies with the decoding power of SUs in tasks involving continuous movements such as scribbling and drawing (e.g., Schwartz et al. 2004). Slow components of the LFP have, by definition, longer cycle times. Therefore despite evidence suggesting they are valuable inputs for decoding straight center-out reaching movements (O'Leary and Hatsopoulos 2006; Rickert et al. 2005), they may degrade relative to SU signals in tasks that involve rapid changes in dynamic and kinematic parameters.

LFP oscillations in the beta range were previously found in the motor cortex (Baker et al. 1997; Donoghue et al. 1998; Murthy and Fetz 1996) and in parietal cortex (Mackay and Mendonça 1995; Scherberger et al. 2005), although their functional role is still under debate. It was suggested (Baker et al. 1999) that motor cortical oscillations promote efficient corticomotor output, whereas asynchronous states are better for the highly demanding computation associated with movement execution. Alternatively, it was suggested (Donoghue et al. 1998) that oscillations reflect general mechanisms of planning and preparatory functions. We found that bouts of beta-range (13–30 Hz) oscillatory activity were frequent in LFP of PPC sites. These oscillations were observed during premovement delay (consistent with Donoghue et al. 1998; Scherberger et al. 2005) and/or during postmovement grip (consistent with Baker et al. 1997). Unlike findings by Rickert et al. (2005), where beta oscillations expressed little directional selectivity, we found that beta oscillations were often selective to target direction and/or object. The different properties of beta oscillations in motor and parietal cortex may suggest that two (or more) different sources of beta oscillations exist in the macaque cortex. Some support for this hypothesis comes from epidural recordings (Mackay and Mendonça 1995), which revealed maximal activity in 20 Hz over motor cortex and maximal activity in 21–29 Hz over medial PPC. Alternatively, differences in task design (e.g., a postcue delay period used in our study) may contribute to this difference in beta-band properties.

Coherent gamma oscillations (30–80 Hz) in the visual cortex were shown to code stimuli and bind features coded in spatially distributed sites (Singer and Gray 1995). More recently, increases in coherence between spikes and LFP in the gamma band were reported to be related to working memory in area LIP (Pesaran et al. 2002) and to target search in area V4 (Bichot et al. 2005). Our data did not contain gamma oscillations in frequency ranges comparable with those reported in the preceding mentioned studies. Instead, a uniform, wide-band (30–100 Hz) increase in gamma-band power was observed throughout the task, and especially during movement. This effect was very different from the relatively narrow peaks in the power spectrum described by Singer and Gray (1995) and others in visual cortex. This wide band increase in gamma power was also reported in motor cortex during reaching (Rickert et al. 2005) and in extrastriate area MT (Liu and Newsome 2006). Furthermore, we found a strong correlation between the specific behavior of the high gamma band and SUs, similar to the finding in MT (Liu and Newsome 2006). However, it is not clear whether this correlation truly reflects synaptic potential dynamics associated with but not tightly time locked to spiking activity. An alternative interpretation for our finding is that selectivity of LFP in the high gamma frequencies to task parameters reflects residuals of the spike waveforms, which also contain energy in frequencies <100 Hz. Indeed, such a wide-band increase in power is *expected* when sharp spike events are low-pass filtered. Further research is required to better examine these alternatives.

Why do different neural signals convey different preferences? Two speculative explanations

A key issue emerging from the results of this study was a noticeable discrepancy between SU and LFP preferences, even when the two signals were recorded from a single electrode. This discrepancy was also evident in the biased distribution of PDs of LFP sites (both evoked and spectral-based tuning curves) as opposed to the uniform distribution of PDs computed for SUs. Similar results were found in other cortical areas such as the cat auditory cortex (Eggermont and Mossop 1998), primary motor cortex (Donchin et al. 2001), and parietal reach region (Scherberger et al. 2005). How can these two neuronal signals carry different messages?

The difference in tuning properties between SU populations and LFPs might be attributed to the sources of the LFP signal. It was shown (Mitzdorf 1985) that LFP reflects a summation of synaptic inputs and not local spiking activity. Hence the LFP might better reflect the events occurring at a station preceding the one where it was recorded and not local computation processes. Furthermore it is possible that a few inhibitory inputs introduce nonlinear effects on SU firing properties, but these contribute very little to the LFP properties. An alternative explanation is that the LFP amplitude is associated with changes in local population synchrony that are too weak to be observed by cross-correlation analyses of SU pairs. Accordingly, LFP preferences would reflect the average preferences of the subpopulation of synchronized neurons, which could be distributed across large cortical areas. A further study of the ongoing interactions among spatially distributed neurons is required to confirm or reject these possibilities.

ACKNOWLEDGMENTS

We are indebted to M. Nakar for invaluable help with construction of the setup, V. Sharkansky for exceptional technical assistance, and G. Goelman for performing numerous MRI scans. We thank R. Drori, Y. Ben-Shaul, and R. Paz for help in the experiments and E. Vaadia for fruitful discussions.

GRANTS

This study was supported in part by a Center of Excellence grant (1564/04) administered by the Israel Science Foundation (ISF), RICH center, and by the German Federal Ministry of Education within the framework of German-Israeli Project Cooperation. Y. Prut was supported by the ISF Grants ISF13355/05 and ISF 555/01.

REFERENCES

Amirikian B, Georgopoulos AP. Directional tuning profiles of motor cortical cells. *Neurosci Res* 36: 73–79, 2000.

Andersen RA, Musallam S, Pesaran B. Selecting the signals for a brain-machine interface. *Curr Opin Neurobiol* 14: 720–726, 2004.

Ashe J, Georgopoulos AP. Movement parameters and neural activity in motor cortex and area 5. *Cereb Cortex* 4: 590–600, 1994.

Baker SN, Kilner JM, Pinches EM, Lemon RN. The role of synchrony and oscillations in the motor output. *Exp Brain Res* 128: 109–117, 1999.

Baker SN, Olivier E, Lemon RN. Coherent oscillations in monkey motor cortex and hand muscle EMG show task-dependent modulation. *J Physiol* 501: 225–241, 1997.

Bichot NP, Rossi AF, Desimone R. Parallel and serial neural mechanisms for visual search in macaque area V4. *Science* 308: 529–534, 2005.

Crammond DJ, Kalaska JF. Differential relation of discharge in primary motor cortex and premotor cortex to movements versus actively maintained postures during a reaching task. *Exp Brain Res* 108: 45–61, 1996.

Donchin O, Gribova A, Steinberg O, Bergman H, Cardoso de Oliveira S, Vaadia E. Local field potentials related to bimanual movements in the primary and supplementary motor cortices. *Exp Brain Res* 140: 46–55, 2001.

Donoghue JP, Sanes JN, Hatsopoulos NG, Gaal G. Neural discharge and local field potential oscillations in primate motor cortex during voluntary movements. *J Neurophysiol* 79: 159–173, 1998.

Eggermont JJ, Mossop JE. Azimuth coding in primary auditory cortex of the cat. I. Spike synchrony versus spike count representations. *J Neurophysiol* 80: 2133–2150, 1998.

Engel AK, Fries P, Singer W. Dynamic predictions: oscillations and synchrony in top-down processing. *Nat Rev Neurosci* 2: 704–716, 2001.

Fisher RA. *Statistical Methods for Research Workers.* Edinburgh, UK: Oliver and Boyd, 1925.

Gardner EP, Ro JY, Debowy D, Ghosh S. Facilitation of neuronal activity in somatosensory and posterior parietal cortex during prehension. *Exp Brain Res* 127: 329–354, 1999.

Georgopoulos AP, Kettner RE, Schwartz AB. Primate motor cortex and free arm movements to visual targets in three-dimensional space. II. Coding of the direction of movement by a neuronal population. *J. Neurosci* 8: 2928–2937, 1988.

Goldberg JA, Rokni U, Boraud T, Vaadia E, Bergman H. Spike synchronization in the cortex/basal-ganglia networks of Parkinsonian primates reflects global dynamics of the local field potentials. *J Neurosci* 24: 6003–6010, 2004.

Jeannerod M. The timing of natural prehension movements. *J Mot Behav* 16: 235–254, 1984.

Kahana MJ, Seelig D, Madsen JR. Theta returns. *Curr Opin Neurobiol* 11: 739–744, 2001.

Lee D, Port NL, Kruse W, Georgopoulos AP. Variability and correlated noise in the discharge of neurons in motor and parietal areas of the primate cortex. *J Neurosci* 18: 1161–1170, 1998.

Liu J, Newsome WT. Local field potential in cortical area MT: stimulus tuning and behavioral correlations. *J. Neurosci* 26: 7779–7790, 2006.

MacKay WA, Mendonça AJ. Field potential oscillatory bursts in parietal cortex before and during reach. *Brain Res* 704: 167–174, 1995.

Mardia KV. *Statistics of Directional Data.* London: Academic, 1972.

Mehring C, Rickert J, Vaadia E, Cardoso de Oliveira S, Aertsen A, Rotter S. Inference of hand movements from local field potentials in monkey motor cortex. *Nat Neurosci* 6: 1253–1254, 2003.

Mitra PP, Pesaran B. Analysis of dynamic brain imaging data. *Biophys J* 76: 691–708, 1999.

Mitzdorf U. Current source-density method and application in cat cerebral cortex: investigation of evoked potentials and EEG phenomena. *Physiol Rev* 65: 37–100, 1985.

Murata A, Gallese V, Kaseda M, Sakata H. Parietal neurons related to memory-guided hand manipulation. *J Neurophysiol* 75: 2180–2186, 1996.

Murthy VN, Fetz EE. Oscillatory activity in sensorimotor cortex of awake monkeys: synchronization of local field potentials and relation to behavior. *J Neurophysiol* 76: 3949–3967, 1996.

O'Leary JG, Hatsopoulos NG. Early visuomotor representations revealed from evoked local field potentials in motor and premotor cortical areas. *J Neurophysiol* 96: 1492–1506, 2006.

Pesaran B, Nelson MJ, Andersen RA. Coherence in dorsal premotor cortex and area MIP during free choice and instructed behaviors. *Soc Neurosci Abstr* 31: 363, 2005.

Pesaran B, Pezaris JS, Sahani M, Mitra PP, Andersen RA. Temporal structure in neuronal activity during working memory in macaque parietal cortex. *Nat Neurosci* 5: 805–811, 2002.

Rickert J, Cardoso de Oliveira S, Vaadia E, Aertsen A, Rotter S, Mehring C. Encoding of movement direction in different frequency ranges of motor cortical local field potentials. *J Neurosci* 25: 8815–8824, 2005.

Roux S, MacKay WA, Riehle A. The pre-movement component of motor cortical local field potentials reflects the level of expectancy. *Behav Brain Res* 169: 335–351, 2006.

Scherberger H, Jarvis MR, Andersen RA. Cortical local field potential encodes movement intentions in the posterior parietal cortex. *Neuron* 46: 347–354, 2005.

Schwartz AB, Moran DW, Reina GA. Differential representation of perception and action in the frontal cortex. *Science* 303: 380–383, 2004.

Singer W, Gray CM. Visual feature integration and the temporal correlation hypothesis. *Annu Rev Neurosci* 18: 555–586, 1995.

Snyder LH, Batista AP, Andersen RA. Coding of intention in the posterior parietal cortex. *Nature* 386: 167–170, 1997.

Stark E, Abeles M. Applying resampling methods to neurophysiological data. *J Neurosci Methods* 145: 133–144, 2005.

Von der Malsburg C, Buhmann J. Sensory segmentation with coupled neural oscillators. *Biol Cybern* 67: 233–242, 1992.